RSC Advances

ROYAL SOCIETY OF CHEMISTRY

www.rsc.org/advances

Remarkable permeability enhancement of polyethersulfone (PES) ultrafiltration membrane by blending cobalt oxide/graphene oxide nanocomposites

Gan Ouyang [1], Asif Hussain[1] Jiebing Li[1], , Dengxin Li[1,*]

[1]College of Environmental Science and Engineering, Donghua University, Shanghai, 201620, China

ABSTRACT: Novel polyethersulfone (PES) ultrafiltration membranes blended with cobalt oxide/graphene oxide (Co_3O_4-GO) nanocomposites were prepared by the phase inversion method. The hybrid membranes were characterized by scanning electron microscopy (SEM), atomic force microscopy (AFM), and energy dispersive spectrometer (EDS). Moreover, the permeability, antifouling, and mechanical and antibacterial properties of the membranes were studied. The experimental results indicated that the pure water flux of the hybrid membrane was improved from 101.1 $L \cdot m^{-2} \cdot h^{-1}$ to 347.9 $L \cdot m^{-2} \cdot h^{-1}$ compared to that of the pristine membrane. In addition, the antifouling performance was investigated by a series of aerobic activated sludge (SV=30%) filtration experiments and the permeability recovery ratio of nanosheet-embedded membrane (81.1%) was significantly increased compared to that of the pristine membrane (55.7%). These significant improvements were mainly ascribed to the enhancement of surface hydrophilicity due to the decrease in the water contact angle from 75.20º to 54.75º and homogenous dispersion of the nanosheets in the polymer matrix. Furthermore, the remarkable improvement in the antibacterial performance (89.8%, against *Escherichia coli*) was also observed. In the study, we blended non-agglomerate metal oxide nanoparticles in polymer matrix to produce the variety of functional material/ membranes for water purification.

Key words: cobalt oxide; graphene oxide; PES membrane; antibacterial

* Corresponding author. Tel.: +86 2167792541; fax: +86 2167792522.
E-mail address: lidengxin@dhu.edu.cn (D. Li).

1. Introduction

Polyethersulfone (PES) has been extensively used in the preparation of ultrafiltration (UF) membranes due to its excellent chemical resistance, good thermal stability, oxidation resistance, and mechanical properties.[1-5] However, the hydrophobic nature of PES ultrafiltration membrane limits its application due to the fouling of membrane surface and pore walls during the separation process.[6] Fouling negatively affects the membrane performance by decreasing water permeability, shortening membrane life and altering membrane selectivity.[6, 7] Consequently, the modification of PES membrane for the higher hydrophilicity is a feasible solution to overcome the issues mentioned above.

Recently, to overcome these concerns, several approaches have been developed, such as blending with amphiphilic copolymer,[8, 9] grafting with hydrophilic monomers,[10, 11] and embedding hydrophilic nanoparticles.[12, 13] In addition, physical incorporation of inorganic additives (such as TiO_2,[14] ZrO_2,[15] and ZnO_2[3]) into polymer matrix have been introduced into the casting solution. These metal oxide nanoparticles were entrapped to increase the hydrophilicity or to improve a specific function of the organic-inorganic hybrid membranes.[16] Shuai Liang et al. applied Nano-ZnO with different dosages ranging from 6.7% to 26.7% (percentage of PVDF weight), as an additive into the membrane matrix for the modification of the internal surfaces of PVDF membrane pores. After series of tests, the modified PVDF membranes showed the significant anti fouling properties.[17]

Cobalt (II,III) oxide (Co_3O_4), as a normal cubic spinel, is composed of face-centered cubic (fcc) arrangement of oxide ions with Co^{2+} ions occupying one-eighth of the tetrahedral sites and Co^{3+} ions occupying half of the octahedral sites.[18] The redox activity of the Co^{2+}/Co^{3+} system makes Co_3O_4 an useful material for various purposes, such as electrochemical applications,[19-21] heterogeneous catalysis,[22,

[23] and gas sensors.[24, 25] Furthermore, due to the excellent performance, cobalt oxide was applied in wastewater treatment. Shukla et al. prepared the nanosized silica-supported Co catalysts for heterogeneous oxidation of phenolic contaminants in waste water.[26] Shi et al. reported the synthesis and synergistic catalysis mechanism of Co_3O_4 and graphene oxide nanocomposite in the heterogeneous activation of peroxymonosulfate (PMS) to generate sulfate radicals for the removal of Azores dye Orange II from water.[27, 28]

Graphene oxide (GO) contains the considerable number of covalently attached oxygen-containing groups, such as hydroxyl, epoxy groups, carbonyl, and carboxyl groups,[29] which make the nanosheets highly hydrophilic. Owing to high hydrophilic nature, high specific surface area (2600 gm^2), and other fascinating chemical properties, GO has been used as an additive for membrane modification.[30, 31] Zinadini et al. prepared polyethersulfone-graphene oxide composite ultrafiltration membranes with the phase inversion method. Compared with the pristine PES membrane, the hybrid membranes exhibited the higher water flux, the higher dye removal capacity and the better fouling resistance.[32] Zhao et al. reported that the permeability, hydrophilicity, and antifouling properties of PVDF/GO composite membranes were improved in long-term membrane bio-reactor tests.[31]

However, the agglomeration of metal oxide nanoparticles is the major drawback in the development of organic-inorganic membrane. Furthermore, previous studies mainly focused on the incorporation of metal particles or GO sheets individually into polymer matrix to produce the modified membrane and antibacterial property was seldom reported. Hence, based on the above issues, the paper aims to investigate the effects of different amounts of embedded Co_3O_4-GO nanocomposite particles on the hydrophilicity, morphology, dispersion, permeability, fouling resistance, and antibacterial property of modified PES membranes.

2. Experimental

2.1. Materials

Polyethersulfone (PES) in the flake form (6020P, Mw= 59,000) provided by BASF Company (Germany) was dried at 100 ºC for 24 h before use. Bovine serum albumin (BSA) (Mw=67,000) and Polyvinylpyrrolidone with the higher molecular weight (PVP K30) were obtained from Sinopharm Chemical Reagent (China). N,N-dimethylacetamide (DMAC) was purchased from Lingfeng Chemical Reagent Company (China). Flake graphite (300 mesh, 99.99%) was supplied by Shanghai Yifan Granphite Co., China. Other reagents including $Co(NO_3)_2 \cdot 6H_2O$, H_2SO_4(98%), $NaNO_3$, $KMnO_4$, and H_2O_2(30%) were of the analytical grade and provided by Sinopharm Chemical Reagent (China).

2.2. Preparation of the Co_3O_4-GO

GO was prepared with natural graphite according to previously reported Hummers and Offeman method.[33] Briefly, GO (400 mg) was dispersed into 240 mL of hexyl alcohol by 3-h sonication. The suspension was centrifuged to remove the sediment and the supernatant liquid was stored for further use. Meanwhile, 6 mM $Co(NO_3)_2 \cdot 6H_2O$ was dissolved into another 160 mL of hexyl alcohol. The mixture was heated to 140 ºC under reflux and vigorous magnetic stirring for 12 h. After the system was cooled to room temperature, the suspension was centrifuged and washed with absolute ethanol and water several times until all the remaining hexyl alcohol and other sundries were removed. Then the suspension was dried in a vacuum oven at 60 ºC for 24 h.[34]

2.3. Preparation of hybrid membranes

Flat sheet porous PES hybrid membranes were prepared according to the phase immersion inversion method. Before preparing the casting solution, 5 wt.% PVP and Co_3O_4-GO blending systems were dispersed in DMAC through 2-h sonication. Then polyethersulfone (15 wt.%) was added into the mixture and stirred at 80 ºC for

approximately 24 h to form a homogenous solution. For all hybrid membranes, the components of casting solutions are shown in Table 1. The homogenous solution was then cast on a glass plate and immediately immersed in a deionized water bath maintained at room temperature. The membranes were peeled off and leached overnight in water to remove trace solvent completely. Then, the membranes were maintained in 50 wt.% glycerol aqueous solution for 24 h to avoid the collapse of the porous structure. The wet membranes were directly used for permeability and fouling resistance measurements after extracting the remaining diluents by washing thoroughly with deionized water. Dry membranes were freeze-dried (Heto PowerDry LL 3000, Gene, USA) and stored for further analysis. The preparation scheme is illustrated in Fig. 1.

2.4. Characterization of Co_3O_4-GO

The structural features and the mineralogy of the graphite and catalysts were studied with X-ray diffraction (XRD) patterns obtained on a RIGAKU XRD instrument by using the filtered Cu Kα radiation with accelerating voltage of 40 kV and the current of 200 mA. The sample was scanned at 2θ from 5º to 90º. The morphology of the synthesized GO and Co_3O_4-GO was observed by scanning electron microscopy (SEM, S-4800, JSM-5600LV, Japan). The size of nanosheets was observed under high resolution transmission electron microscopy (FE-HRTEM, JEOL, JEM-2100F), and the sample was prepared by dispersing a small amount of dry powder in ethanol.

2.5. Characterization of hybrid membranes

2.5.1. Porosity and mean pore radius

The membrane porosity ε (%) was defined as the volume of the pores of the membrane divided by the total volume of the membrane. It is usually calculated as:[35]

$$\varepsilon = \frac{(w_1 - w_2)/dw}{(w_1 - w_2)/dw + w_2/dp} \times 100\%, \quad (1)$$

where w_1 is the weight of the wet membrane (kg); w_2 is the weight of the dry membrane (kg); dw is the pure water density (998.00 kg·m^{-3}); dp is the polymer density. Δp is the PES polymer density (1370 kg·m^{-3}).

Mean pore radius r_m (m) was determined by filtration velocity method. According to Guerout-Elford-Ferry Equation, r_m is calculated as:[35]

$$r_m = \sqrt{\frac{(2.9-1.75\varepsilon)\times 8\eta l Q}{\varepsilon \times A \times \Delta P}}, \quad (2)$$

where η is the water viscosity (8.90 × 10^{-4} Pa·S); l is the membrane thickness (m); Q is the volume of permeate water per unit time (m^3·s^{-1}); A is the effective area of the membrane (m^2); ΔP is the operational pressure (1.00 × 10^5 Pa).

2.5.2. Tensile strength and elongation

The mechanical performance of the membranes was evaluated with a material testing machine (H5K-S, UK) with the stretching rate of 20 mm/min at room temperature. Each specimen was cut into pieces (5×1 cm^2) and each sample was tested for 3 times. Tensile extension and tensile strain at break were then measured to investigate the effect of modification on the mechanical strength.

2.5.3. Static contact angle

The hydrophilicity of the membrane was evaluated according to the surface contact angle at room temperature. Five microliters of water was dropped on the top surface of a dry membrane from a micro syringe with a stainless steel needle. The static contact angle was obtained with the average value of 5 measurements at different places on the membrane sample.

2.5.4. Permeability and rejection ratio of hybrid membranes

The membrane permeability properties were tested in a laboratory ultrafiltration (UF) unit at a pressure of 0.10 MPa and room temperature. The system contains a filtration cell (MSC300, China) with the volume capacity of 300 mL and the filter area of 37.37 cm^2. The pressure required in the system is supplied via compressed air.

After the membrane was fixed, the stirred cell and solution reservoir were fed with deionized water. Each membrane was initially pressurized for 30 min at 0.10 MPa until there was no variation in permeate flux before use. The water flux (J_{w1}) is

calculated by measuring filtration time at a fixed volume under constant transmembrane pressure. The water flux J_{w1} ($L \cdot m^{-2} \cdot h^{-1}$) is calculated as:

$$J_{w1} = \frac{V}{At}, \quad (3)$$

where V(L), A(m^2), and t(h) represent the volume of permeated water, the membrane filtering area, and permeation time, respectively.

The same unit was fed with 1.0 $mg \cdot mL^{-1}$ BSA (molecular weight = 67,000) solution for the rejection experiment at the stirring speed of 300 rpm and room temperature. Then, the concentration of both feed solution (C_f) and permeate solution (C_p) was determined by an ultraviolet-visible spectrophotometer (UV-7504) at 280 nm (XIN MAO Instruments Co., Ltd., China) after maintaining the operating pressure of 0.1 MPa for 2 h. The BSA rejection (R) is calculated as:

$$R = \frac{C_f - C_p}{C_f} \times 100\%, \quad (4)$$

where C_f($mg \cdot L^{-1}$) and C_p ($mg \cdot L^{-1}$) are the protein concentrations of the feed solution and permeate solution, respectively.

2.5.5. Surface morphology and roughness

The cross-section morphologies of hybrid membranes were observed by scanning electron microscopy (SEM, S-4800, JSM-5600LV, Japan). Before analysis, membrane samples were cleaned with deionized water and then cut into small pieces. After drying, the samples were sputtered with a thin gold layer to become electrically conductive.

The membrane surface morphology and roughness were analyzed by atomic force microscopy (Vecco, Nano scope 3D, USA) under the tapping mode in air. The images and roughness parameters (Ra, Rq) were determined through the AFM analysis software (Nano scope software version 5004-210-000). Approximately, membrane samples with the area of 1 cm^2 were fixed with a specimen holder and the area of 5 μm x 5 μm were scanned. The surface roughness parameters were reflected in terms of the average roughness (Ra) and the root mean square of the Z data (Rq) within the scanning area of 5 μm x 5 μm.

The elemental composition was determined through energy dispersive X-ray spectroscopy (EDS). EDS (IE300X, Oxford, UK) analysis was conducted at several points in the region. The determination values were averaged to obtain the representative results.

2.5.6. Antifouling performance

Membrane simulated crossflow obtained by constant vigorous stirring in a dead-end filtration device connected with an air compressor pump and solution reservoir was designed to characterize the filtration performance of the membranes. The membrane was firstly pre-compacted at the trans-membrane pressure of 0.1 MPa with deionized water until a steady-state flux (J_{w1}) was observed. Subsequently, the attenuation experiments were conducted with aerobic activated sludge (SV=30%) from an aeration tank as the feed to achieve quick and severe fouling on the membranes. The permeability of the aerobic activated sludge (J_{wA}) was also recorded after the constant trans-membrane pressure of 0.1 MPa was maintained for 60 min. Then, the fouling membrane was washed with deionized water for 30 min in the filtration direction and then the post-cleaning pure water flux (J_{w2}) was measured under the same pressure. The above process represents one filtration cycle. The flux recovery ratio (*Frr*) was determined and calculated as:[36, 37]

$$Frr = \frac{J_{w2}}{J_{w1}} \times 100\% . \quad (5)$$

A higher value of *Frr* indicates the preferable antifouling performance of the ultrafiltration membranes.

To analyze the fouling process in detail, several resistance ratios are defined to describe the antifouling performance of the blended membranes. The total fouling ratio (R_t), reversible fouling ratio (R_r), and irreversible fouling ratio (R_{ir}) were respectively determined as follows:

$$R_t = 1 - \frac{J_{wA}}{J_{w1}} \times 100\% , \quad (6)$$

$$R_r = \frac{J_{w2} - J_{wA}}{J_{w1}} \times 100\% , \quad (7)$$

$$R_{ir} = \frac{J_{w1} - J_{w2}}{J_{w1}} \times 100\% . \quad (8)$$

The ratio R_t is the sum of R_r and R_{ir}.

2.6. Antibacterial properties

For quantitatively analyzing the antibacterial activities of the membranes, antibacterial rate against *E. coli* was employed. Each membrane was cut into pieces with the size of 5 mm × 5 mm. All the experimental instruments were sterilized by autoclaving at 121 ºC for 20 min, respectively. The actual number of cells for each experiment was determined with the standard serial dilution method. Various membranes (100 mg) were added into the 5 mL of solution and 10^6 CFU/ml of *E. coli* was inoculated and then put in a shaker under the speed of 250 r/min at 37 ºC. After 18 h, 0.5 mL of bacterial suspension was absorbed and then added into 4.5 mL of normal saline until its concentration became 10^{-4} of the original value. Then, 0.1 mL of dilution solution was spread onto Lactose Broth (LB) culture medium and all the plates were incubated at 37 ºC for 24 h. The numbers of the colonies on the plates were determined according to the plate count method. The antibacterial rate (R_A) was calculated as:

$$R_A = (\frac{A - B}{A}) \times 100\% , \quad (9)$$

where A is the number of bacterial colonies on the plates from the dilution solution of the pristine membrane and B is the number of bacterial colonies on the plates from the dilution solution of the hybrid membrane.

3. Results and Discussion

3.1. Characterization of Co_3O_4-GO nanocomposites

XRD is an effective method for investigating the crystalline properties of a synthesized material. The structural properties of Co_3O_4-GO were analyzed by XRD and compared with bare GO. As shown in Fig.2, the GO pattern shows a characteristic peak at 2θ = 9.32º , which corresponds to an interlayer spacing of 0.95 nm and

indicates the presence of oxygen-containing functional groups which play an important role in improving the hydrophilicity of hybrid membrane formed during oxidation. The pattern of Co_3O_4-GO shows the reflection planes (002), (003), (004), (005), (006), (007), (008), and (009) at 18.91º, 31.20º, 36.72º, 44.70º, 59.23º, 64.92º, and 77.12º, respectively. These diffraction lines provide the clear definite of the formation of GO and Co_3O_4 and were in good agreement with previous results.[27, 36]

The surface morphologies of the synthesized GO and Co_3O_4-GO composites were observed from the SEM images (Fig. 3). The inner surface of GO was quite smooth, while the Co_3O_4 attached to GO appeared in the form of bright dots which were uniformly decorated and firmly anchored on the wrinkled GO layers with high density. The size of Co_3O_4 particles in the composite was approximately less than 10 nm.[28] Additionally, the TEM image shows that the size of Co_3O_4-GO composites was approximately less than 100 nm (Fig. 4).

3.2. Porosity and mean pore radius

The pore size could be determined by the interpenetration velocity of the water-solvent during the phase inversion. As shown in Fig. 3, when the dosage of Co_3O_4-GO was increased from 0 to 2.0 wt.%, the mean pore size of as-prepared membranes was increased from 30.7 nm to 57.2 nm. This gradual increase is caused by the high hydrophilicity of nanocomposite (Co_3O_4-GO) and it is well consistent with the previous result.[38] However, the porosity was not significantly changed by the mixing nanosheets and only a slight increase was observed. A similar observation result after blending of nano-ZnO particle in PVDF membrane was previously reported.[39]

3.3. Mechanical properties of hybrid membranes

Tensile strength is an important parameter to investigate the mechanical properties of a membrane. Fig. 4 reveals that compared to the pristine membrane, hybrid membranes showed the improved tensile strength after the nanosheet content was increased from 0.5 wt.% to 1.0 wt.%. However, with the increase of the embedded

amount, the tensile strength gradually declined and even became less than that of the pristine one. This phenomenon is in consistent with the theory that an organic-inorganic hybrid membrane has the flexibility of an organic membrane and the stiffness of an inorganic membrane.[40] The phenomenon may be interpreted as follows. There are plenty of oxygen-containing functional groups on the surface of Co_3O_4-GO composites. Crystals might be formed partly due to the static regularity of their planar construction and the intermolecular force between Co_3O_4-GO nanosheets and PES. With the increase of nanosheet content, the intermolecular force declined and the crystallinity might be ruined because the higher amount of nanosheets were collocated irregularly and caused the static hindrance. Thus, the tensile strength declined continually.

3.4. Static contact angle

The hydrophilicity of the membrane surface was investigated according to water contact angle, which also reflects the natural wettability of the membrane. The larger contact angle means that the membrane surface is more hydrophobic. The average static contact angle significantly declined from 75.20º to 54.75º when Co_3O_4-GO was embedded into the casting solution (Fig. 5). The water contact angle was decreased with the increase in the Co_3O_4-GO amount and showed the lowest value at 2.0 wt.%, indicating the remarkably improved hydrophilicity of as-prepared modified membrane (Fig. 5). This phenomenon was probably caused by the hydrophilicity of the nanosheets which were intrinsically linked with plenty of hydrophilic groups, such as –OH, -COOH, and C-O-C. During the phase inversion process, the nanosheets were brought to the top layer due inter-sheet diffusion and exchange process between solvent and non-solvent. Consequently, the particles were brought to the top surface and exposed in water (Fig. 6). Meanwhile, the larger dosage of Co_3O_4-GO indicates the more hydrophilic groups decorated on the membrane top surface, which represent the lower static contact angle and interface energy.[37]

3.5. Permeability and rejection ratio

Pure water flux and rejection ratio were analyzed to investigate the effect of Co_3O_4-GO nanosheets on the PES membrane performance. From Fig. 7, the pure water permeability was promoted significantly after the nanosheets were embedded into the casting solution. The results showed the significant increase in the permeability (365 $L \cdot m^{-2} \cdot h^{-1}$) of the modified membrane compared to the pristine membrane (101.1 $L \cdot m^{-2} \cdot h^{-1}$) prepared from 1.5 wt.% nanosheets in the casting solution. This may be attributed to the hydrophilicity of the Co_3O_4-GO, which migrates to the top surface of the membrane during the phase inversion process. Simultaneously, the modified membranes were endowed with the advantageous pore size.

However, the water flux of hybrid membranes did not show any increase with increase in the dosage of nanosheets. Actually, the flux reached a peak when the content of nanosheets was 1.5 wt.%; the flux decreased when the content of nanosheets was increased above 1.5 wt.%. The rejection parameter curve of prepared membranes for BSA is also plotted in Fig. 4. The rejection ratio of the membrane was about 95% of that of the modified membrane, and it was slightly decreased when the embedding content of nanosheets increased to the optimum value. This decreasing trend is well consistent with the previous study of incorporating isocyanate-treated graphene oxide for membrane modification.[41] The trend can be interpreted as follows. Although excessive nanosheets increased the hydrophilicity, the decline in the pore size and pore blocking with the high concentration of the nanosheets discussed below caused the decline in the permeability and had positive impacts on maintaining the high rejection ratio.

3.6. Microscopic morphologies

SEM was employed to observe the cross-section morphologies of prepared membranes with different Co_3O_4-GO contents (Fig. 8). After the phase inversion process, typical asymmetric structures, such as dense skin layer, finger-like porous sub-layer, and macrovoid structure, were observed in these six images of the prepared membranes.

Interestingly, as shown in the SEM images (Fig. 8), the incorporation of nanosheets in matrix significantly modified the pore structure of prepared membranes. With the increase in the dosage of introduced nanosheets, the sub-layer of the prepared membranes turned thinner and the size of macrovoid became smaller. However, the permeability of the cross-section structure turned better. The above changes may be responsible for the combination of the significantly improved flux and the high rejection ratio of modified membranes. The results are highly consistent with the permeability and rejection performance obtained in related experiments. The change in the lateral pore structure may be interpreted as follows. The hydrophilicity of Co_3O_4-GO increases the mass transfer rate[42] and the viscosity of the casting solution due to the smoother exchange process between the solvent and the non-solvent during the phase inversion. However, some lateral pore structure appeared when excessive nanosheets were embedded into the matrix (Fig. 8(f)). The change in the lateral pore structure might obstruct many pore channels and cause the decrease in the permeability of modified membranes.

Atomic force microscopy (AFM) was also employed to investigate the surface roughness of the prepared membranes. Fig. 9 illustrates the three dimensional surface morphologies of the membranes. The average roughness (*Ra*) and the root mean square roughness (*Rq*) in Table 2 are calculated with the scanning area of 5 μm x 5 μm. The average roughness (*Ra*) of the pure PES membrane and hybrid membrane was respectively 12.4 and 8.5, indicating that the surface of the hybrid membrane was apparently smoother. The change was caused by the incorporation of Co_3O_4-GO nanosheets into the polymeric matrix through filling membrane pores and the similar behavior of GO/PVDF membrane was reported by Xia et al.[43] In addition, the increase in roughness was caused by the more Co_3O_4-GO nanosheets accumulated on the membrane surface. However, under the optimum dosage (2.0 wt.%), the observed average roughness of the hybrid membrane was lower than that of the pure membrane. The result is consistent with the previous result that the surface roughness is increased after the more additive is embedded into membrane.[32, 44] It is well known that a

membrane with the smoother surface has the higher fouling resistance capability,[38] which affects the antifouling performance during the ultrafiltration process.

The dispersion quality as well as the existence of nanosheets in the membrane section was analyzed by energy dispersive spectrometer (EDS) surface scanning. The presence of Co element confirmed the existence of Co_3O_4-GO in the membrane section. In the elemental distribution map (Figs. 10(a) and 10(c)), purple dots represent the element of cobalt, indicating that the nanosheets are uniformly distributed in the polymer matrix. Additionally, as shown in Figs. 10(b) and 10(d), the content of cobalt in PES-2.0 was approximately twice as that of PES-1.0 and equal to the designed content. As expected, a highly dispersed and homogeneous system of organic and inorganic phases at the nanoscale level might be achieved by ultrasonic dispersion and mechanical stirring during the preparation of the casting solution. Besides, the uniform dispersion of nanosheets could markedly improve the stability of the membrane and protect the particles from being leached in wastewater treatment process.

3.7. Antifouling performance

The filtration performance of a membrane depends on its antifouling property. The filtration performance leads to various complications, such as the blockage or plugging of pores within the membrane as well as the concentration polarization and cake layers formed on the surface.[45] Membrane fouling is mainly determined by the adsorption and deposition of proteins on the membrane surface and the entrapment of proteins in the pores. The poor antifouling property is mainly caused by the hydrophobic behaviors of membrane surfaces.[46]

The antifouling performances of the hybrid membranes and pristine membrane were analyzed by measuring the water flux and recovery ratio. Two cyclic filtration tests were performed with aerobic activated sludge (SV=30%) from an aeration tank as a model. The flux behaviors of hybrid membranes with different contents of nanosheets were depicted in Fig. 11. The permeability of all the membranes declined dramatically in the initial filtration stage. It is proposed that some sludge in the feed will be deposited or absorbed on the membrane surface to form cake layer, thus

causing the drop of flux within the few minutes after initiating the performance operation. Moreover, the membrane with 1.5 wt.% Co_3O_4-GO complex showed the most significant flux decline. The steady-state permeate fluxes of the aerobic activated sludge (J_{wA}) for the pristine membrane and the hybrid membrane embedded with 1.5 wt.% nanosheets were respectively 46.7 $L \cdot m^{-2} \cdot h^{-1}$ and 200.4 $L \cdot m^{-2} \cdot h^{-1}$. When the nanosheet content was increased above 1.5 wt.%, the flux was decreased. It is obvious that the hybrid membranes can maintain the higher flux in ultrafiltration process.

To further investigate the antifouling property during the filtration process in detail, *Frr*, *Rt*, *Rir*, and *Rr* of the investigated membranes are summarized in Fig. 12. It is obvious that the *Frr* of pristine membrane (55.75%) is lower than that of modified membranes. With the increase in the content of nanosheets, the *Frr* showed an upward tendency until the embedding content of 1.0 wt.% and then dropped slightly. The larger *Frr* indicates the better antifouling property of a membrane. The observed trend of *Frr* is quite comparable to that of other inorganic particles, such as silica[37] and TiO_2 [12] employed for the modification of PES membranes.

The total fouling ratio (R_t), which is the sum of reversible fouling ratio (R_r) and irreversible fouling ratio (R_{ir}), is 53.77% for the pristine membrane, which is higher than that of all the modified membranes. Additionally, the value of *Rir* is the observed decrease in the flux of pure water before and after the filtration of a protein solution. Due to strong adsorption of protein molecules on the surface or entrapment of protein molecules in pores, the *Rir* of the pristine membrane and the membrane PES-1.5 were respectively 44.23% and 18.89%, demonstrating that the antifouling property could be effectively promoted by Co_3O_4-GO nanosheets modification.

These results may be caused by two factors. Firstly, the hydrophilicity of the modified hybrid membranes decreases the interaction between the membrane surface and sludge, the sorption content on the surface, and pore blocking.[47, 48] Secondly, the smoother surface of the hybrid membranes decreases trapping and aggregation of the foulants in the membrane pores and valleys of the surface.

Cobalt oxide is a toxic substance. In order to determine the leached cobalt oxide during filtration process, inductively coupled plasma mass spectrometry (ICP-MS) was applied to analyze the filtered liquid after every cycle of the operation experiments. Moreover, BSA rejection experiment was conducted again to verify whether the additive had been removed or not after five circles. According to the verification results, cobalt had not been found in the filtered liquid and the rejection ratio was still higher than 94% as before, which indicated that cobalt had not been leached from the hybrid membrane and that the modified membranes could be applied safely in water purification.

3.8. Antibacterial performance

The experiment result of antibacterial performance shows that the quantity of *E. coli* colonies in the hybrid membrane was significantly decreased compared to that in the pristine membrane. Moreover, the antibacterial rate of hybrid membranes increased dramatically with the increase in the content of embedded Co_3O_4-GO (Fig. 13, Table 4). The results indicated that antibacterial effect had been introduced successfully by blending various contents of Co_3O_4-GO in PES membrane. Grapheme-based nanomaterials could inhibit the growth of *E. coli*.[49] As shown in Fig. 13, when the addition dosages of GO, Co_3O_4, and Co_3O_4-GO are 1.0 wt.%, the antibacterial rates of PES-bGO and PES-Co_3O_4 membrane are respectively 43.7% and 63.3%, which are lower than that of Co_3O_4-GO (84.4%) hybrid membranes. Hence, the antibacterial effect of as-prepared hybrid membrane reflects the synergistic action between GO and Co_3O_4.

The antibacterial mechanism of the hybrid membranes could be interpreted as follows. The irreversible damages of bacterial cells could be induced after directly contacting with graphene because the membrane stress induced on bacterial cells resulted in the destruction of cell structures.[50] In the study, plenty of nanosheets on the surface of the hybrid membranes caused the antibacterial action of hybrid membranes. Moreover, cobalt oxide could catalyze the generation of free radical in the light,

which also damaged important biological macromolecules in cells and inhibited bacterial growth and reproduction.

4. Conclusions

PES membranes incorporated with Co_3O_4-GO nanosheets were prepared by using the immersion phase inversion method. The nanosheets incorporated into polymer matrix played a favorable role in the characteristics of PES membranes. The influences of the incorporated nanosheets were summarized below:

(1) The hybrid membranes exhibited the higher mean pore size and porosity and the better mechanical properties than the pristine membrane.

(2) The static contact angle declined from 75.20º (PES-0) to 54.75º (PES-2.0), which represented a significant enhancement of hydrophilicity.

(3) The pure water flux of hybrid membranes was increased by 344% (PES-1.5) compared to that of the pristine and the rejection ratio of BSA was still more than 94%. The characterization of morphologies confirmed these results.

(4) The hybrid membranes showed the better fouling resistance and the higher recovery ratio after sludge filtration performance and the antibacterial rate of the hybrid against *E. coli* was up to 89.8%.

Regarding the obtained permeability, antifouling performance and antibacterial properties, the optimum concentration of nanosheets in casting solution was found to be 1.5 wt.%. The study showed that Co_3O_4-GO nanosheets-modified membranes had the potential application in water purification.

Acknowledgement

This work was financially supported by Specialized Research Fund for the Doctoral Program of Senior Education of China (Grant No. 20130075110006).

References

1. F. Jin, W. Lv, C. Zhang, Z. Li, R. Su, W. Qi, Q.-H. Yang and Z. He, *RSC Advances*, 2013, **3**, 21394-21397.

2. S. Li, G. Liao, Z. Liu, Y. Pan, Q. Wu, Y. Weng, X. Zhang, Z. Yang and O. K. C. Tsui, *Journal of Materials Chemistry A*, 2014, **2**, 12171-12176.
3. X. Li, J. Li, B. Van der Bruggen, X. Sun, J. Shen, W. Han and L. Wang, *RSC Advances*, 2015, **5**, 50711-50719.
4. L. Liu, D. Y. W. Di, H. Park, M. Son, H.-G. Hur and H. Choi, *RSC Advances*, 2015, **5**, 7340-7348.
5. L.-J. Zhu, L.-P. Zhu, Y.-F. Zhao, B.-K. Zhu and Y.-Y. Xu, *Journal of Materials Chemistry A*, 2014, **2**, 15566-15574.
6. S. Qing, S. Yanlei, Z. Shiping, L. Chao, Z. Yanyan and J. Zhongyi, *Journal of Membrane Science*, 2007, **303**, 204-212.
7. H. Susanto and M. Ulbricht, *Journal of Membrane Science*, 2009, **327**, 125-135.
8. M. Peyravi, A. Rahimpour, M. Jahanshahi, A. Javadi and A. Shockravi, *Microporous and Mesoporous Materials*, 2012, **160**, 114-125.
9. A. Rahimpour and S. S. Madaeni, *Journal of Membrane Science*, 2007, **305**, 299-312.
10. M. N. Abu Seman, M. Khayet and N. Hilal, *Desalination*, 2012, **287**, 19-29.
11. A. Rahimpour, *Desalination*, 2011, **265**, 93-101.
12. V. Vatanpour, S. S. Madaeni, A. R. Khataee, E. Salehi, S. Zinadini and H. A. Monfared, *Desalination*, 2012, **292**, 19-29.
13. V. Vatanpour, S. S. Madaeni, L. Rajabi, S. Zinadini and A. A. Derakhshan, *Journal of Membrane Science*, 2012, **401**, 132-143.
14. Q. Wang, Z. Wang, J. Zhang, J. Wang and Z. Wu, *RSC Advances*, 2014, **4**, 43590-43598.
15. Y. Zhang, L. Wang and Y. Xu, *Chemical Engineering Journal*, 2015, **260**, 258-268.
16. J. M. Arsuaga, A. Sotto, G. del Rosario, A. Martinez, S. Molina, S. B. Teli and J. de Abajo, *Journal of Membrane Science*, 2013, **428**, 131-141.
17. L. Shuai, X. Kang, M. Yinghui and H. Xia, *Journal of Membrane Science*, 2012, **394-395**, 184-192.
18. S. Vetter, S. Haffer, T. Wagner and M. Tiemann, *Sensors and Actuators B-Chemical*, 2015, **206**, 133-138.
19. S. Park and S. Kim, *Electrochimica Acta*, 2013, **89**, 516-522.
20. R. B. Rakhi, W. Chen, M. N. Hedhili, D. Cha and H. N. Alshareef, *Acs Applied Materials & Interfaces*, 2014, **6**, 4196-4206.
21. X. Zhang, Y. Zhao and C. Xu, *Nanoscale*, 2014, **6**, 3638-3646.
22. F. Jiao and H. Frei, *Angewandte Chemie-International Edition*, 2009, **48**, 1841-1844.
23. H. Tueysuez, Y. J. Hwang, S. B. Khan, A. M. Asiri and P. Yang, *Nano Research*, 2013, **6**, 47-54.
24. T. Wagner, J. Roggenbuck, C.-D. Kohl, M. Fröba and M. Tiemann, in *Studies in Surface Science and Catalysis*, eds. S. Q. Y. T. Dongyuan Zhao and Y. Chengzhong, Elsevier, 2007, vol. Volume 165, pp. 347-350.
25. H. Yamaura, K. Moriya, N. Miura and N. Yamazoe, *Sensors and Actuators B-Chemical*, 2000, **65**, 39-41.
26. P. Shukla, H. Sun, S. Wang, H. M. Ang and M. O. Tade, *Separation and Purification Technology*, 2011, **77**, 230-236.
27. P. Shi, X. Dai, H. Zheng, D. Li, W. Yao and C. Hu, *Chemical Engineering Journal*, 2014, **240**, 264-270.

28. P. Shi, R. Su, S. Zhu, M. Zhu, D. Li and S. Xu, *Journal of Hazardous Materials*, 2012, **229**, 331-339.
29. A. Lerf, H. Y. He, M. Forster and J. Klinowski, *Journal of Physical Chemistry B*, 1998, **102**, 4477-4482.
30. L. Jaewoo, C. Hee-Ro, W. Young June, L. Kibaek, L. Chung-Hak, H. H. Lee, K. In-Chul and L. Jong-min, *Journal of Membrane Science*, 2013, **448**, 223-230.
31. C. Zhao, X. Xu, J. Chen, G. Wang and F. Yang, *Desalination*, 2014, **340**, 59-66.
32. S. Zinadini, A. A. Zinatizadeh, M. Rahimi, V. Vatanpour and H. Zangeneh, *Journal of Membrane Science*, 2014, **453**, 292-301.
33. W. S. Hummers and R. E. Offeman, *Journal of the American Chemical Society*, 1958, **80**, 1339-1339.
34. T. He, D. R. Chen and X. L. Jiao, *Chemistry of Materials*, 2004, **16**, 737-743.
35. N. Li, C. Xiao, S. An and X. Hu, *Desalination*, 2010, **250**, 530-537.
36. T. Battumur, S. B. Ambade, R. B. Ambade, P. Pokharel, D. S. Lee, S.-H. Han, W. Lee and S.-H. Lee, *Current Applied Physics*, 2013, **13**, 196-204.
37. M. Sun, Y. Su, C. Mu and Z. Jiang, *Industrial & Engineering Chemistry Research*, 2010, **49**, 790-796.
38. L.-Y. Yu, Z.-L. Xu, H.-M. Shen and H. Yang, *Journal of Membrane Science*, 2009, **337**, 257-265.
39. J. Hong and Y. He, *Desalination*, 2014, **332**, 67-75.
40. Y. Liang, Z. Yatao, Z. Bing, L. Jindun, Z. Haoqin and S. Chunhua, *Journal of Membrane Science*, 2013, **447**, 452-462.
41. H. Zhao, L. Wu, Z. Zhou, L. Zhang and H. Chen, *Physical Chemistry Chemical Physics*, 2013, **15**, 9084-9092.
42. V. Vatanpour, S. S. Madaeni, R. Moradian, S. Zinadini and B. Astinchap, *Journal of Membrane Science*, 2011, **375**, 284-294.
43. S. Xia and M. Ni, *Journal of Membrane Science*, 2015, **473**, 54-62.
44. X. Chang, Z. Wang, S. Quan, Y. Xu, Z. Jiang and L. Shao, *Applied Surface Science*, 2014, **316**, 537-548.
45. A. G. Fane and C. J. D. Fell, *Desalination*, 1987, **62**, 117-136.
46. C. H. Koo, A. W. Mohammad, F. Suja and M. Z. M. Talib, *Desalination*, 2012, **287**, 167-177.
47. M. Chunxia, S. Yanlei, S. Mengping, C. Wenjuan and J. Zhongyi, *Journal of Membrane Science*, 2010, **350**, 293-300.
48. C. Wenjuan, S. Yanlei, Z. Lei, S. Qing, P. Jinming and J. Zhongyi, *Journal of Membrane Science*, 2010, **348**, 75-83.
49. M. Jizhen, Z. Jintao, X. Zhigang, Y. Yu and X. S. Zhao, *Journal of Materials Chemistry*, 2011, **21**, 3350-3352.
50. S. Liu, T. H. Zeng, M. Hofmann, E. Burcombe, J. Wei, R. Jiang, J. Kong and Y. Chen, *Acs Nano*, 2011, **5**, 6971-6980.

Table 1 The compositions of casting solutions.

Membrane types	PES (wt.%)	PVP (wt.%)	Co3O4-GO (wt.%)
PES-0	15	5	0
PES-0.5	15	5	0.5
PES-1.0	15	5	1.0
PES-1.5	15	5	1.5
PES-2.0	15	5	2.0

Table 2 Surface roughness parameters of Co_3O_4-GO hybrid membranes resulted from the analysis of three randomly chosen AFM images.

Membrane types	Roughness parameters	
	Ra (nm)	Rq (nm)
PES-0	12.4±1.4	15.2±1.4
PES-0.5	6.6±1.3	8.5±1.5
PES-1.0	10.6±1.1	13.7±1.2
PES-1.5	11.1±1.5	13.9±1.6
PES-2.0	12.2±1.1	15.4±1.2

Table 3 Antifouling properties of hybrid membranes with different Co_3O_4-GO embedding contents.

Membrane types	FRR (%)	R_t (%)	R_r (%)	R_{ir} (%)
PES-0	71.02	30.46	1.48	28.98
PES-0.5	73.03	60.42	33.45	26.97
PES-1.0	79.13	58.34	37.47	20.87
PES-1.5	71.26	40.10	31.15	28.74
PES-2.0	66.43	62.18	28.61	33.57

Table 4 Antibacterial rates of tested membranes against *E. coli*.

Membrane types	The numbers of bacterial colonies (cfu)	Antibacterial rate (%)
PES-0	128	-
PES-0.5	43	66.4
PES-1.0	20	84.4
PES-1.5	17	86.7
PES-2.0	13	89.8
PES-bGO	72	43.7
PES-Co_3O_4	47	63.3

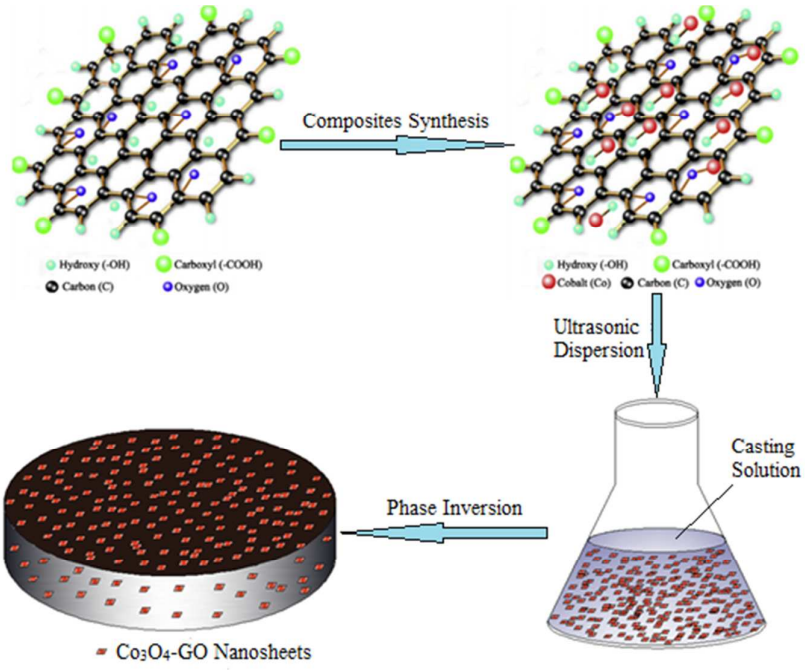

Fig.1 The process scheme of preparation of hybrid ultrafiltration membrane

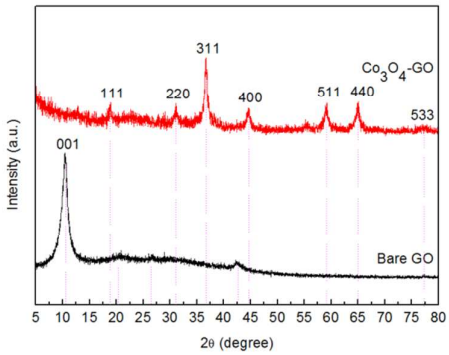

Fig. 2 XRD patterns of bare GO and Co_3O_4-GO composites

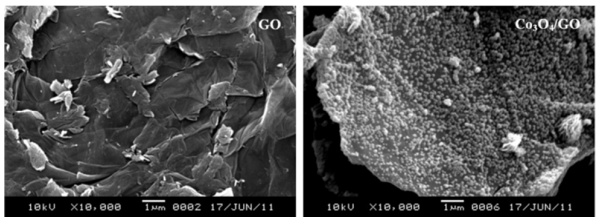

Fig. 3 SEM images of the synthesized GO and Co_3O_4-GO composites

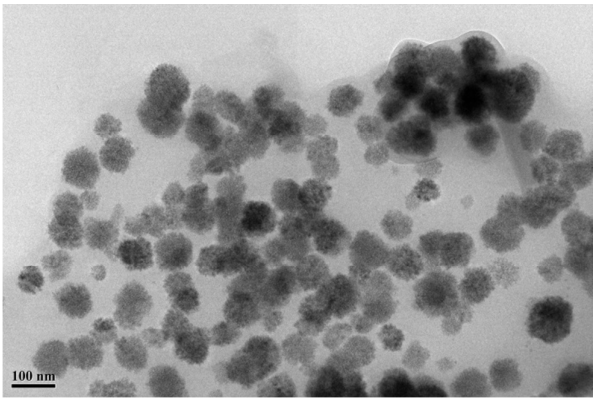

Fig. 4 TEM images of synthesized Co_3O_4-GO composites

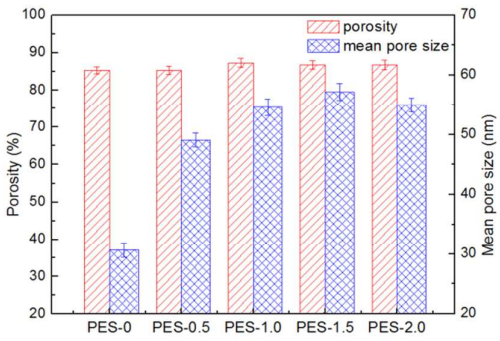

Fig. 5 Porosity and mean pore size of membranes

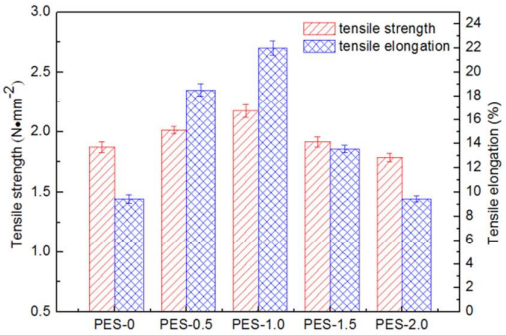

Fig.6 Measurement of tensile strength and elongation of membranes

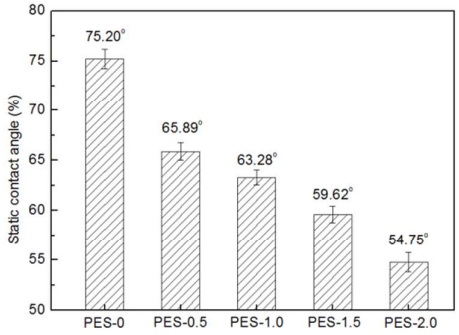

Fig.7 The effect of nanosheets content on static contact angle of hybrid membrane hybrid membranes

Fig.8 The photograph of top and bottom surface of 2.0 wt.% Co_3O_4-GO hybrid membrane

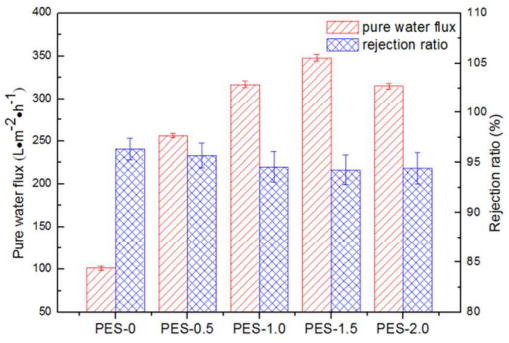

Fig.9 The effects of different content of nanosheets on permeability and rejection rate of membranes

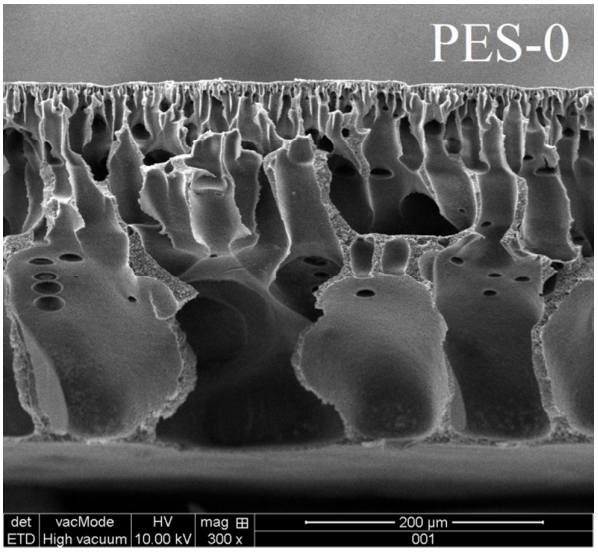

(a)

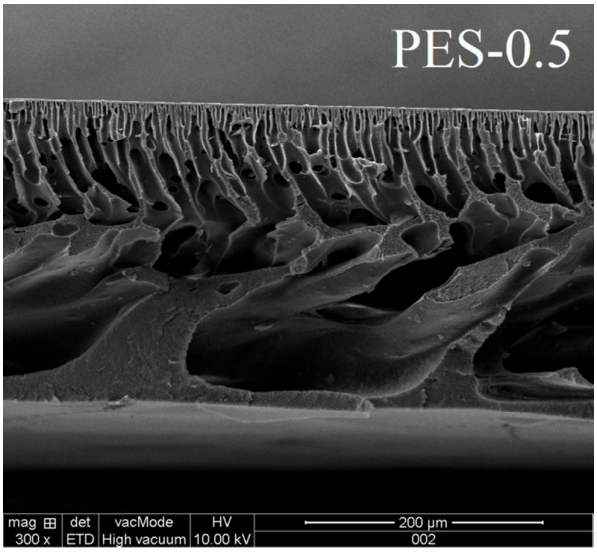

(b)

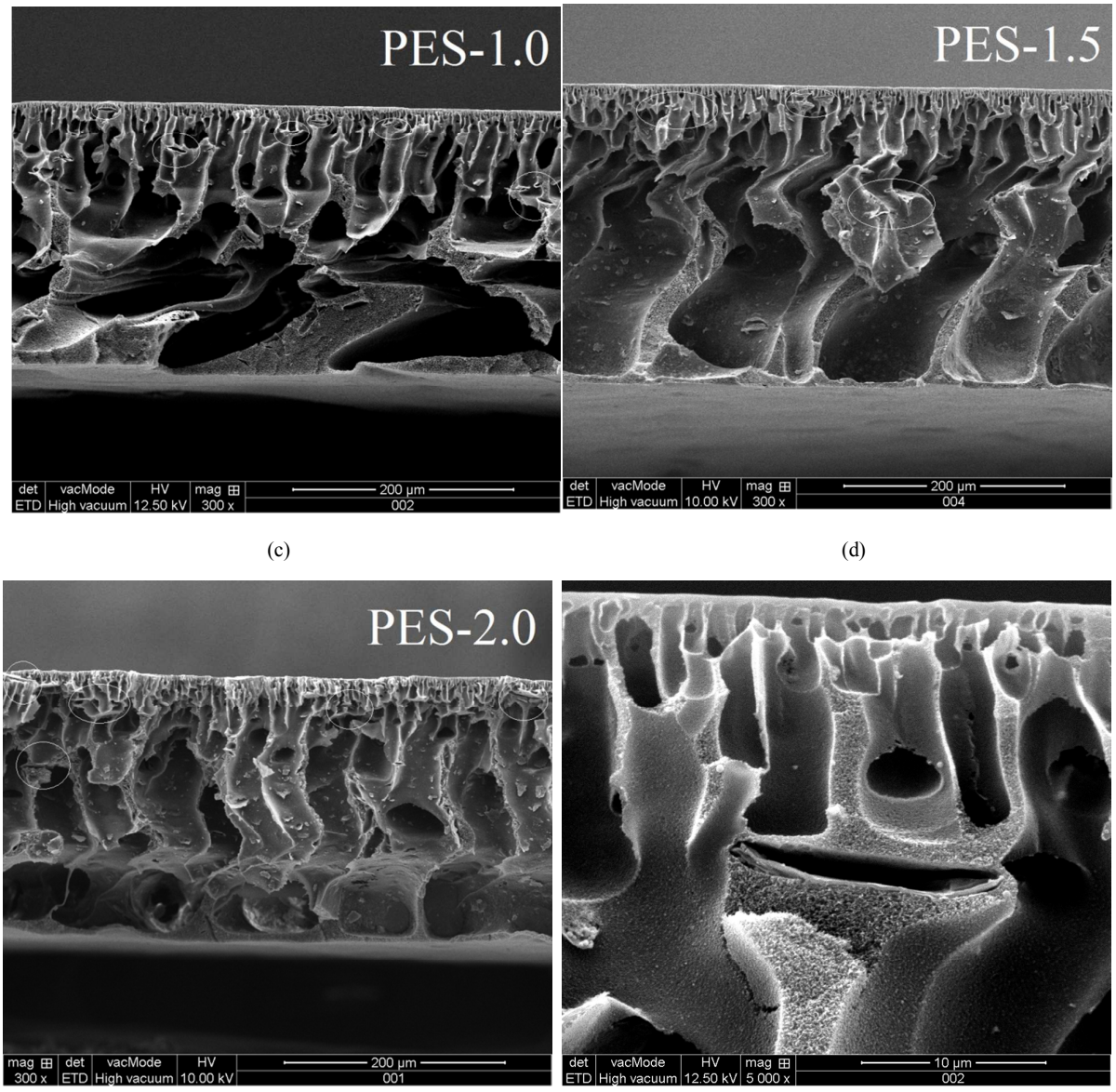

Fig.10 FE-SEM images of cross-section of different content of nanosheets hybrid membranes at the magnification of 300x: a) 0.0 wt%; b) 0.5 wt%; c) 1.0 wt%; d) 1.5wt%; e) 2.0wt%; f) skin layer at the magnification of 5000x

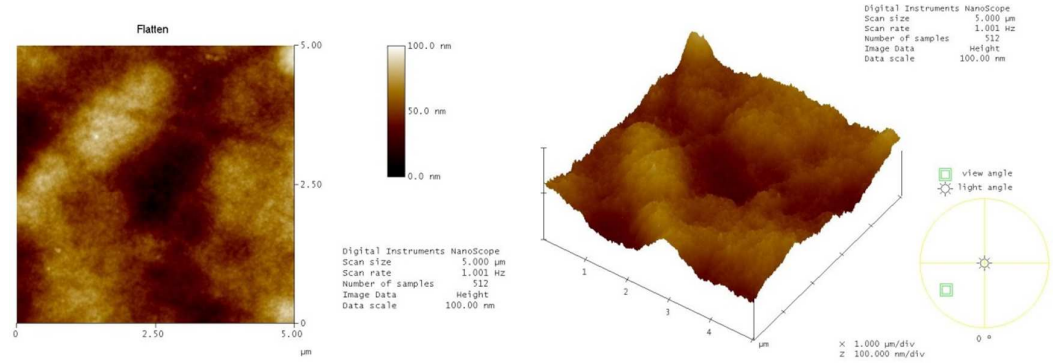

(a)

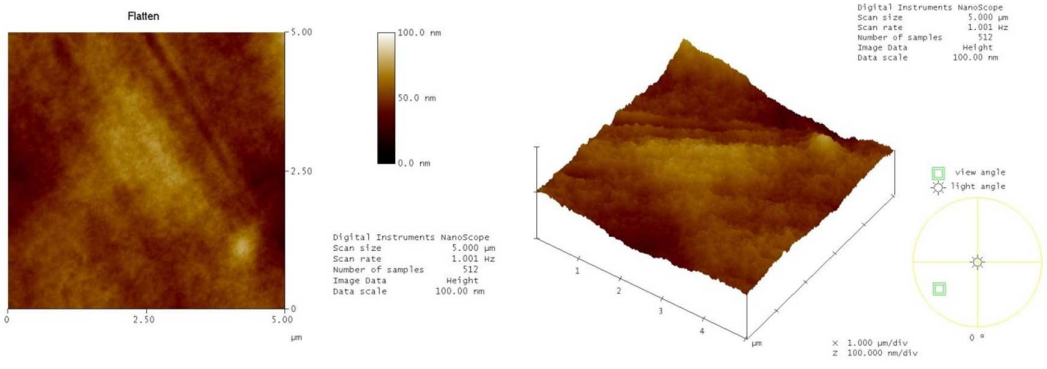

(b)

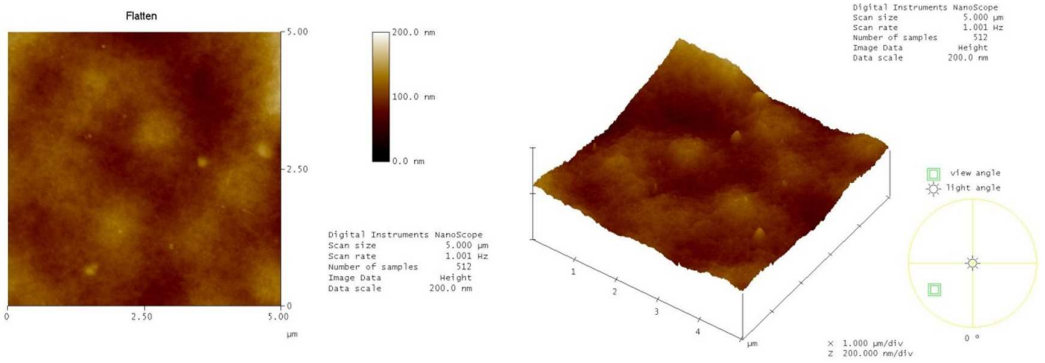

(c)

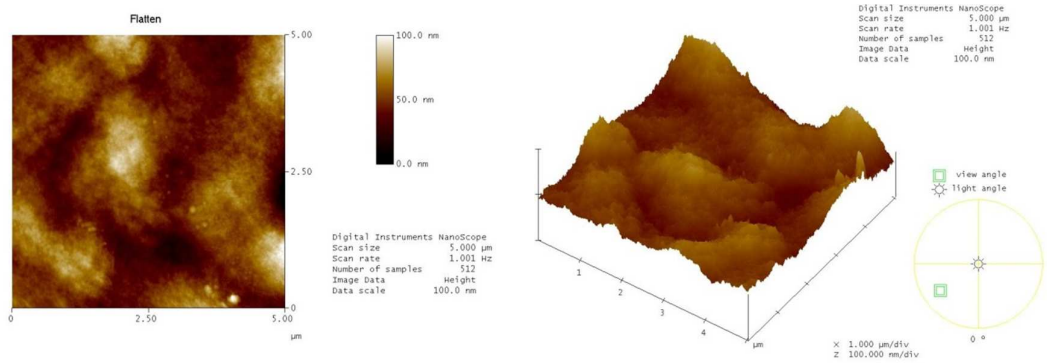

(d)

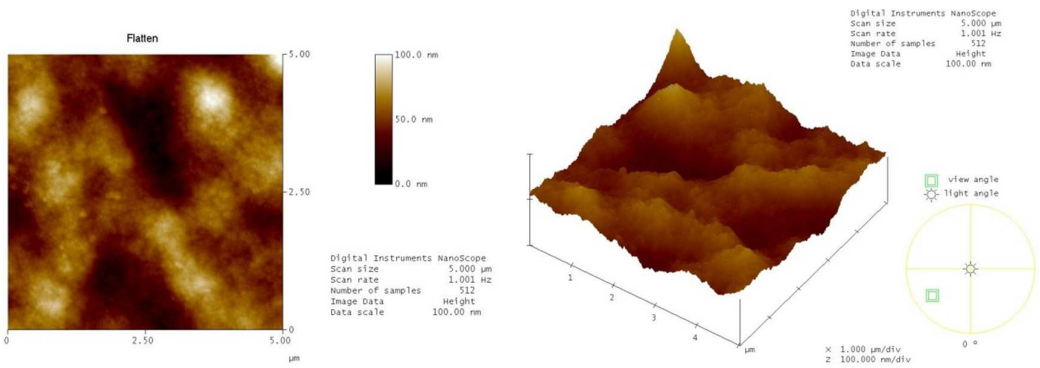

(e)

Fig.11 AFM images of prepared membranes upper surfaces (the scanning area of 5µm x 5µm): a) PES-0; b) PES-0.5; c) PES-1.0; d) PES-1.5; e) PES-2.0

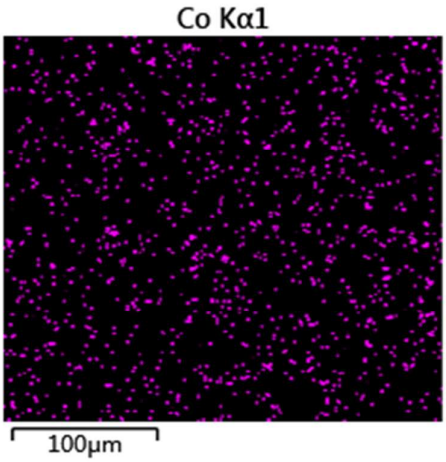

(a)

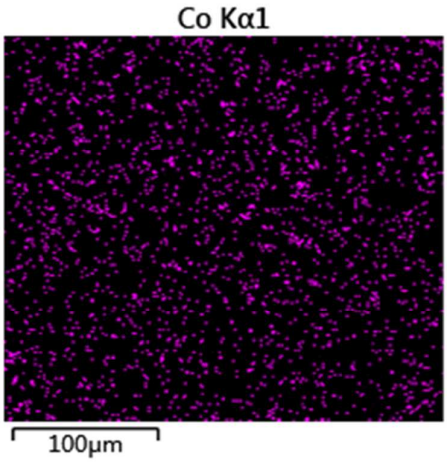

(c)

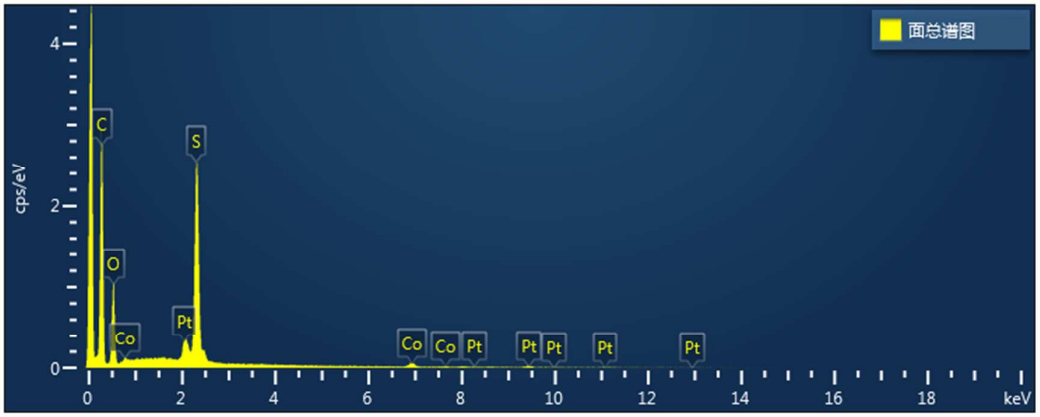

(b)

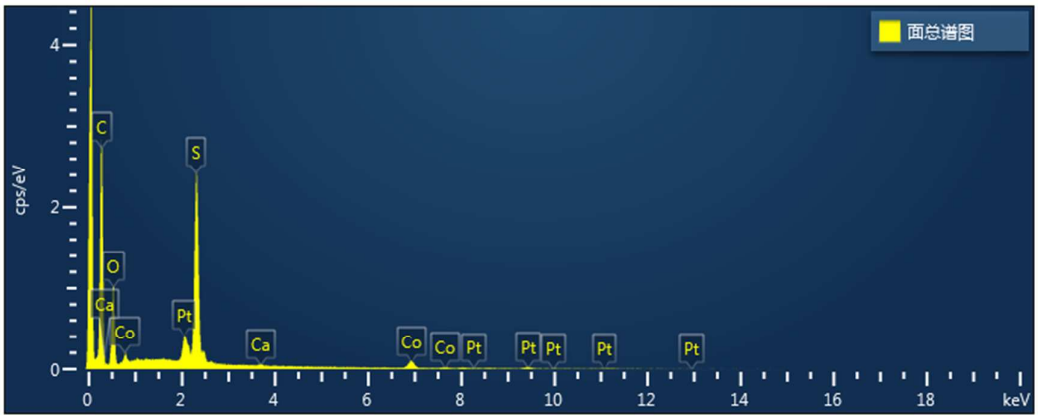

(d)

Fig.12 EDS images of different content of nanosheets hybrid membranes: a, b) 1.0 wt.%; c, d) 2.0 w.t%

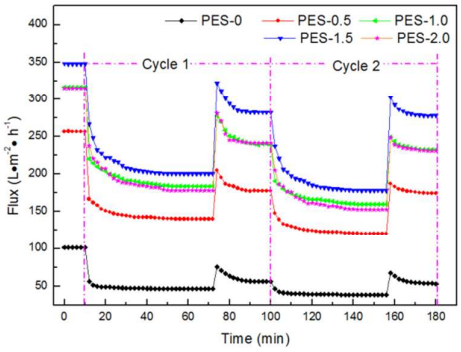

Fig. 13 Flux behavior of prepared membranes under two cycles of sludge (SV=30%) filtration measurements

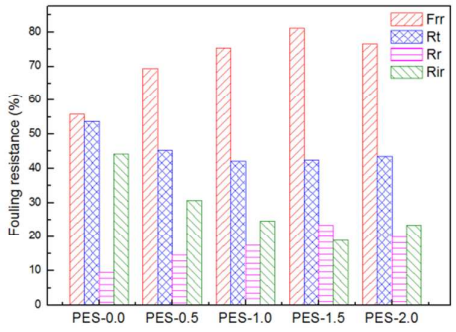

Fig. 14 comparison of Frr, Rt, Rr and Rir of prepared membranes under two cycles of sludge (SV=30%) filtration

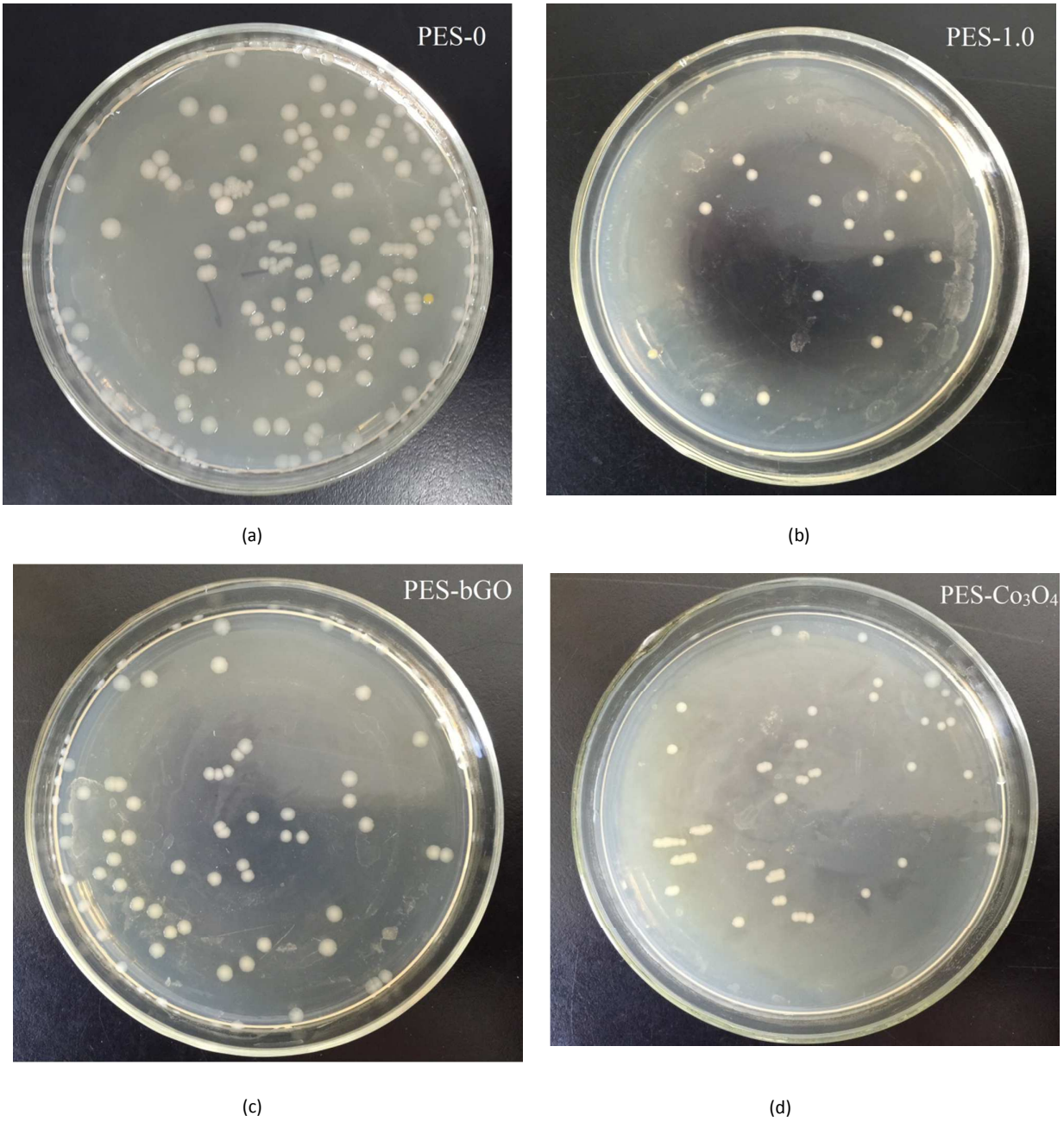

Fig.15 measurement of antibacterial property by the antibacterial rate: a)PES-0; b) PES-1.0; c) PES-bGO; d) PES-Co_3O_4